Electronic Supplementary Information (ESI)

Sustainable direct current powering triboelectric nanogenerator via intent asymmetrical design

Hanjun Ryu,[a‡] Jeong Hwan Lee,[a‡] Usman Khan,[a] Sung Soo Kwak,[a] Ronan Hinchet[a] and Sang-Woo Kim*[a,b]

[a]School of Advanced Materials Science and Engineering, Sungkyunkwan University (SKKU), Suwon, 16419, Republic of Korea

[b]SKKU Advanced Institute of Nanotechnology (SAINT), Sungkyunkwan University (SKKU), Suwon, 16419, Republic of Korea

*Correspondence to : kimsw1@skku.edu (S.-W. Kim)

†Hanjun Ryu and Jeong Hwan Lee contributed equally to this work

Supplementary Note 1. Effect of different material-based rotators on TENG

Generally, in the freestanding rotation type triboelectric nanogenerator (TENG), a single material-based rotator is used and the material selection of the rotator and stator determines the amount of contact electrification charges on the rotator.[1-3] Typically, the density of the triboelectric charge on the rotator is two times higher than that of the opposite charge on the stator due to an unequal contact surface area between the rotator and the stator.[4] The triboelectric charges on the surface of the rotator electrostatically induce the opposite charges on the electrodes, thereby causing charges flow among the electrodes. Therefore, the triboelectric charges generated on the rotator are closely related to the rotator material and it is also used to determine the output performance. In order to improve the TENG performance, we designed and utilized different material-based rotators and a polytetrafluoroethylene (PTFE) freestanding layer-based stator (see Supplementary Figure 2). When a single mono cast (MC) nylon rotator was rotated on the stator, the PTFE freestanding layer was negatively charged due to the contact electrification between the MC nylon rotator and the PTFE freestanding layer. Due to the unequal contact surface area, half of $\sigma_{\text{MC nylon}}$ is induced on one electrode, and the other electrode has positive induced charges for electric balance. While the MC nylon rotator rotates on the other electrode, the negative induced charges flow through the external circuit and generate around 130 V (see Supplementary Figure 2a). When a single PTFE rotator is rotated on the stator, the PTFE freestanding layer was positively charged due to the contact electrification between the PTFE rotator and the PTFE freestanding layer. Because of the unequal contact surface areas, half of σ_{PTFE} is induced on one electrode, and the other electrode has negative induced charges for electric balance. While the PTFE rotator rotates on the other electrode, the density of the triboelectric charge of the PTFE rotator is relatively smaller than the density of the MC nylon rotator,[5] so that the positive induced charges flow through the external circuit at 35 V (see Supplementary Figure 2b). In order to increase the surface triboelectric charges of the rotator, we fabricate a rotator structure composed of strips of two friction materials, PTFE and MC nylon, which are radially interlaid between each other (see Supplementary Figure 2c). While the MC nylon is positively charged, the PTFE freestanding layer will be negatively charged and the surface potential of the PTFE will increase. When the PTFE rotator comes into contact with the positively charged PTFE freestanding layer with a higher surface potential than the PTFE rotator, the PTFE rotator is easily negatively charged and the PTFE freestanding layer is positively charged.[6] As a result, the PTFE freestanding layer is both positively and negatively charged, and these charges neutralize each other. The surface charge density of the rotator and stator is also enhanced due to the contact de-electrification and long-range effects between neighboring rotor materials.[7] As a result, the enhanced induced charge of the stator electrode increases and generates about 200 V (see Supplementary Figure 2c). Supplementary Figure 2d-2f showed the finite element method (FEM) simulations of the multiple PTFE and MC nylon patterned rotator based TENG. The surface charge of the PTFE (σ_{PTFE}) and MC nylon ($\sigma_{MC\ nylon}$) are equal and opposite; the freestanding layer's surface is charged with a net of ($\sigma_{PTFE} + \sigma_{MC\ nylon}$) 0. Therefore, the multiple PTFE and MC nylon patterned rotator are harvested more efficiently than the single material based rotator.

Supplementary Note 2. Calculation of the equivalent galvanostatic current

The equivalent galvanostatic current (I_{eg}) is calculated by equation (1)

$$I_{eg} = \frac{C \times \Delta V}{\Delta t} \tag{1}$$

Where C is capacitance of the capacitor, ΔV is the voltage change during the charging or discharging time (Δt). According to the Fig. 3c experimental result, the C is 1 mF, ΔV is 0.70 V, Δt is 10 sec. Therefore, equivalent galvanostatic current (I_{eg}) is 70 μA.

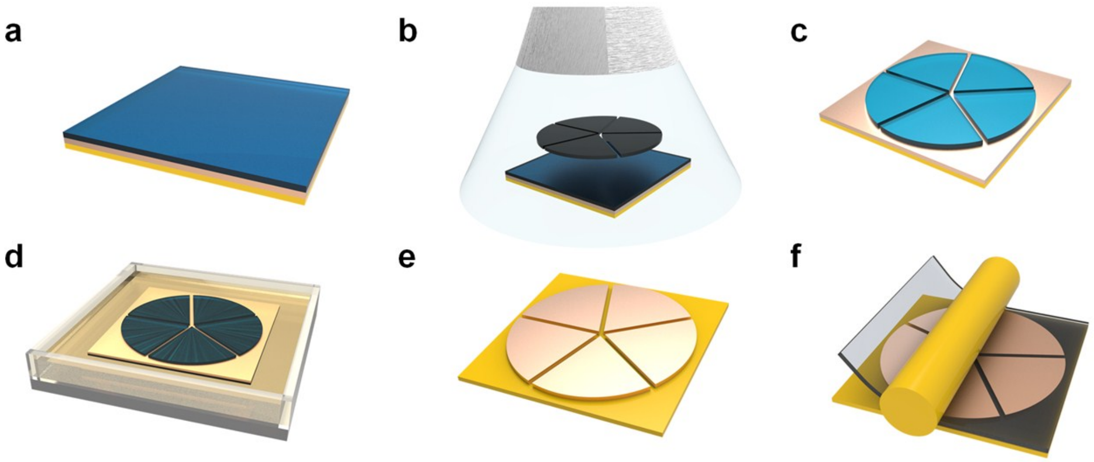

Supplementary Figure 1. Schematic description of fabricating a 5-phase stator. (a) Preparation of commercially available positive photo-reactive (PR) printed circuit board (PCB) (GD1530, SME Trading Co., LTD). **(b)** Exposed ultraviolet (UV) light to mask/PCB. **(c)** Developed PR exposed to UV light. **(d)** Etch exposed oxide using ferric chloride solution. **(e)** Removed remaining PR and leansing device. **(f)** PTFE film attached to the PCB.

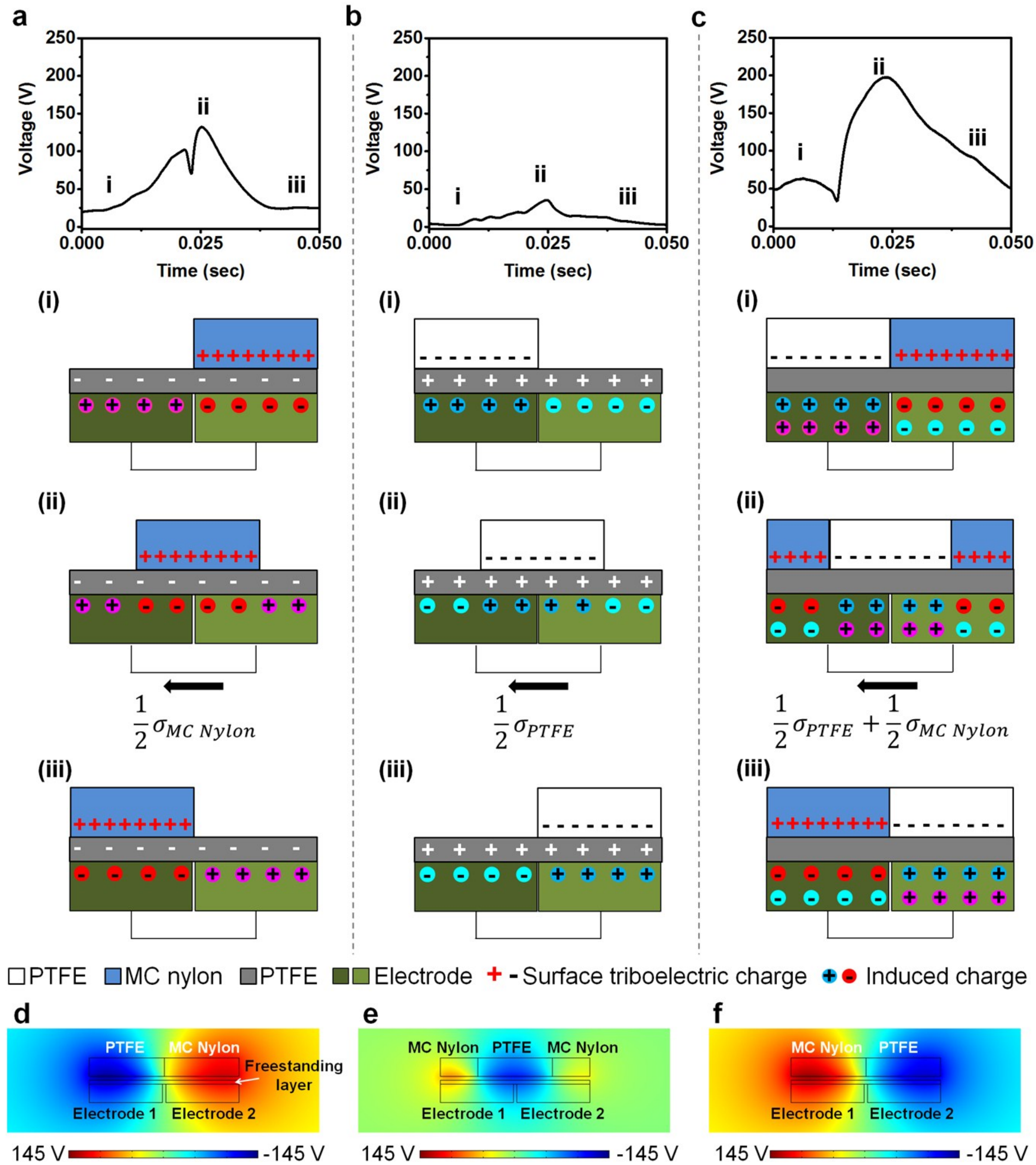

Supplementary Figure 2. Design and output performance of different material-based rotators and PTFE freestanding layer-based stator (a) Single MC-nylon rotator based TENG. **(b)** Single PTFE rotator based TENG. **(c)** Multiple PTFE and MC nylon patterned rotator based TENG. **(d)** The FEM simulation of the multiple PTFE and MC nylon patterned rotator based TENG at (i) state, **(e)** at (ii) state, and **(f)** at (iii) state.

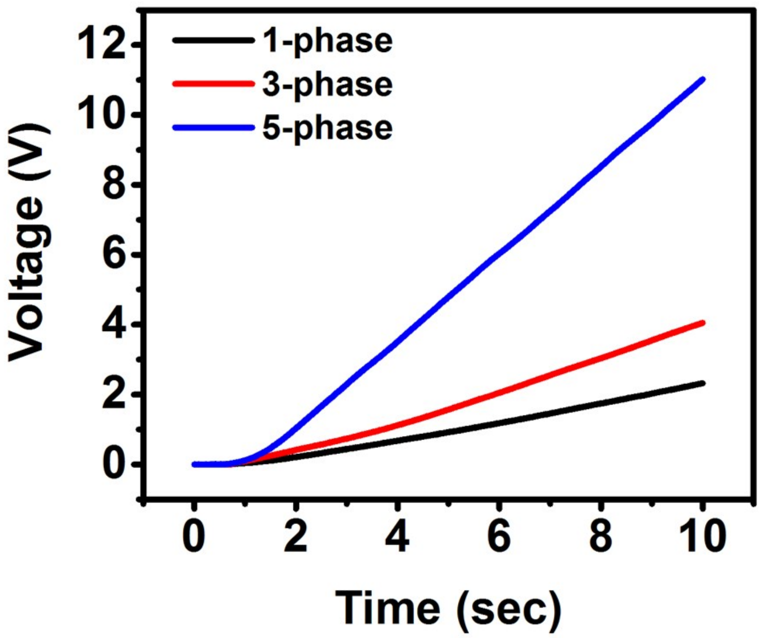

Supplementary Figure 3. Comparison 10 μF capacitor charging behavior by the MP-TENGs.

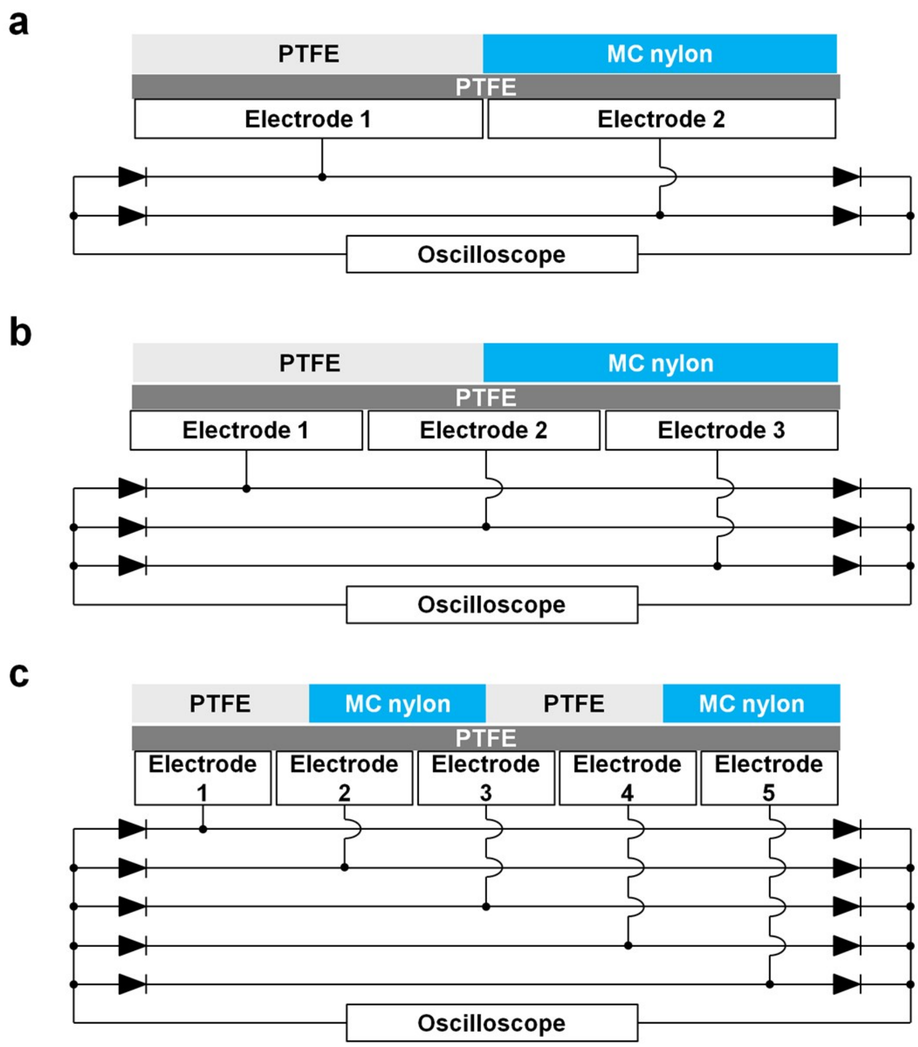

Supplementary Figure 4. Multi-phase management circuit diagram of the MP-TENG. (a) Circuit diagram of single phase TENG. **(b)** Circuit diagram of 3-phase TENG. **(c)** Circuit diagram of 5-phase TENG.

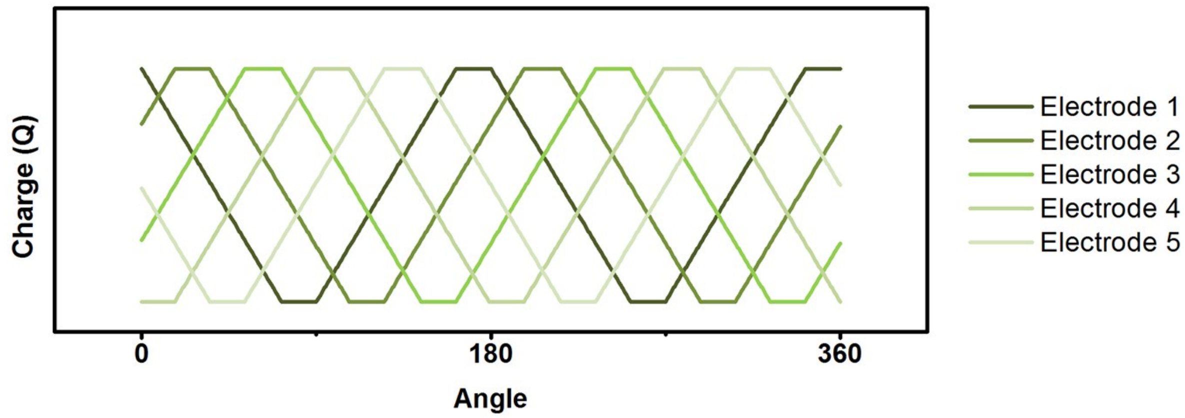

Supplementary Figure 5. Schematic graph of triboelectric induced charge depending on rotating angle of rotator in an ideal condition.

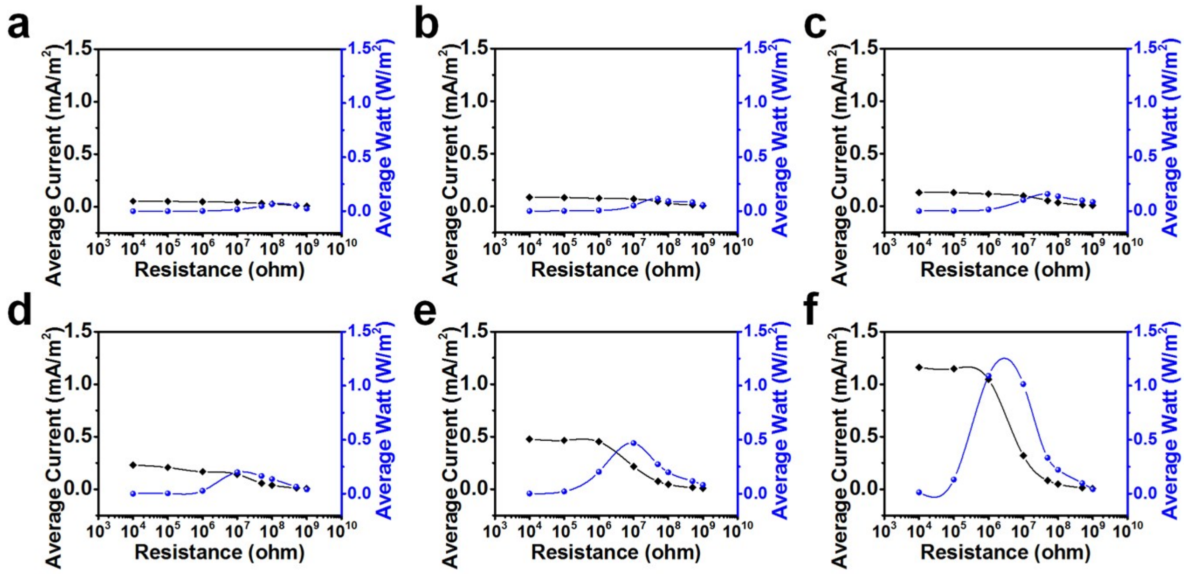

Supplementary Figure 6. 5-phase TENGs output current and power performances at the rotator speed 240 RPM as a function of the external load resistance. **(a)** Output performance of 1 segmentation TENG. **(b)** Output performance of 2 segmentations TENG. **(c)** Output performance of 3 segmentations TENG. **(d)** Output performance of 6 segmentations TENG. **(e)** Output performance of 9 segmentations TENG. **(f)** Output performance of 18 segmentations TENG.

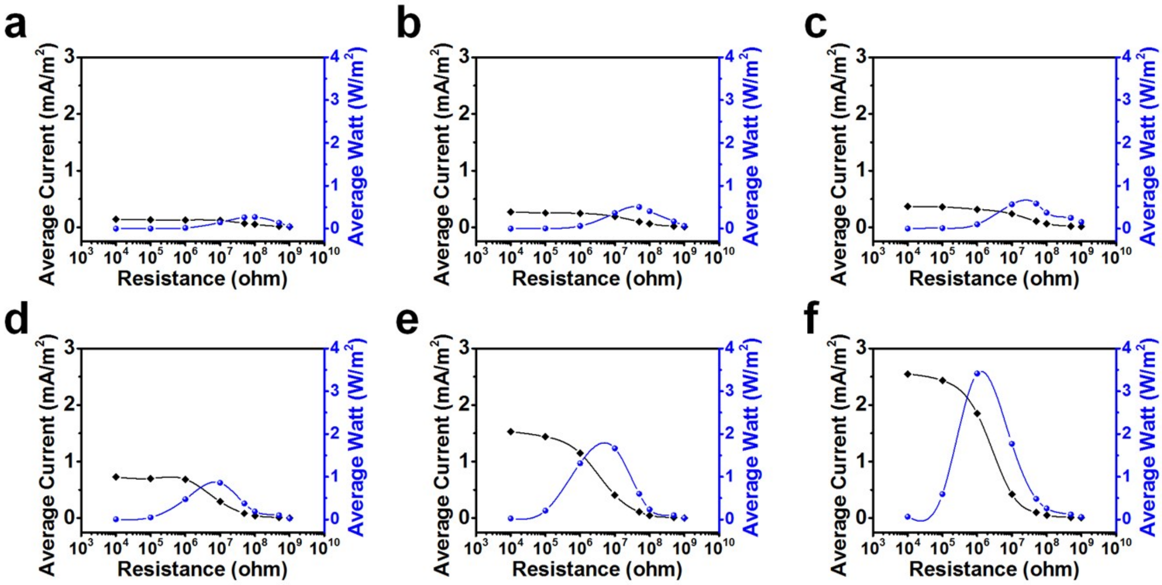

Supplementary Figure 7. 5-phase TENGs output current and power performances at the rotator speed 600 RPM as a function of the external load resistance. **(a)** Output performance of 1 segmentation TENG. **(b)** Output performance of 2 segmentations TENG. **(c)** Output performance of 3 segmentations TENG. **(d)** Output performance of 6 segmentations TENG. **(e)** Output performance of 9 segmentations TENG. **(f)** Output performance of 18 segmentations TENG.

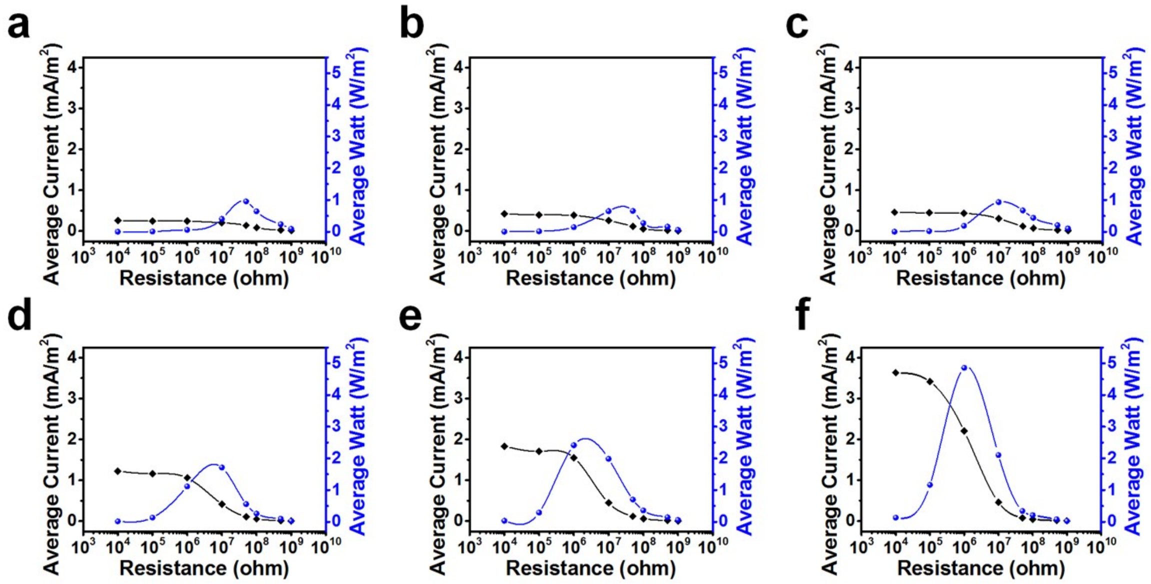

Supplementary Figure 8. 5-phase TENGs output current and power performances at the rotator speed 920 RPM as a function of the external load resistance. **(a)** Output performance of 1 segmentation TENG. **(b)** Output performance of 2 segmentations TENG. **(c)** Output performance of 3 segmentations TENG. **(d)** Output performance of 6 segmentations TENG. **(e)** Output performance of 9 segmentations TENG. **(f)** Output performance of 18 segmentations TENG.

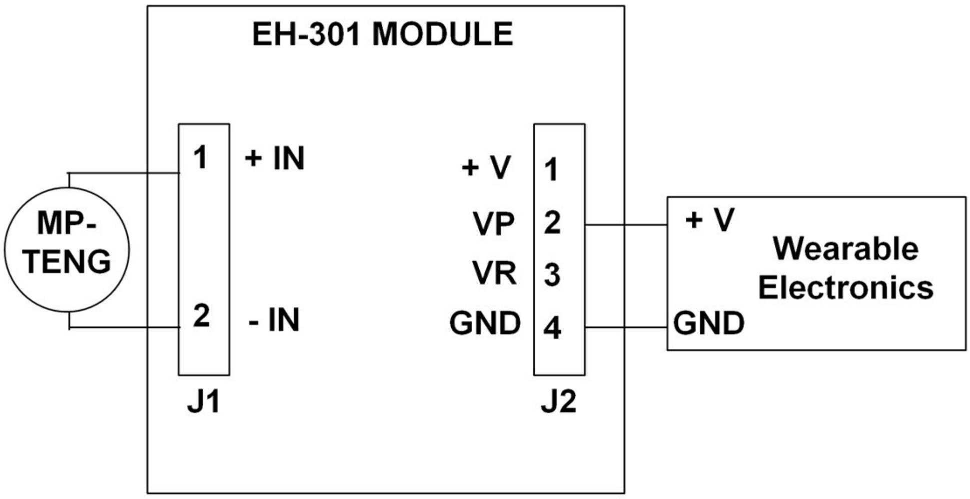

Supplementary Figure 9. Energy management circuit system for studying charging Mi-band property.

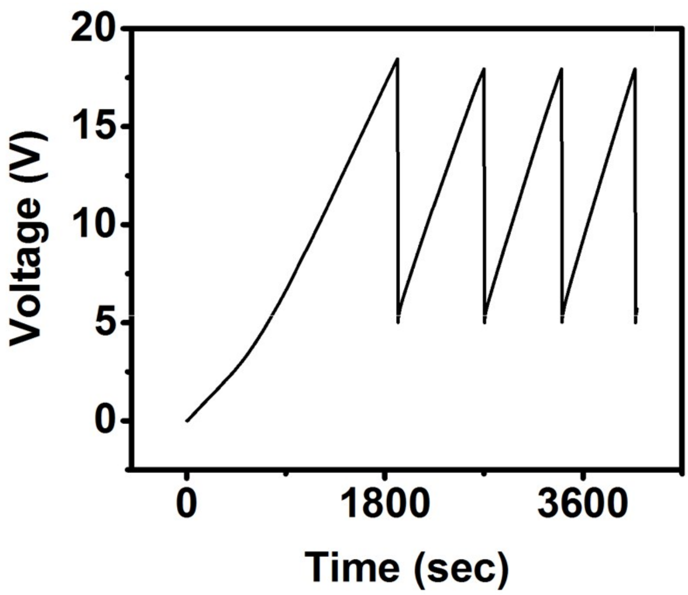

Supplementary Figure 10. Demonstration of the periodically operates the temperature sensor.

Supplementary References

1. Z. Wen, J. Chen, M.-H. Yeh, H. Guo, Z. Li, X. Fan, T. Zhang, L. Zhu and Z. L. Wang, *Nano Energy*, 2015, **16**, 38-46.
2. S. Chen, N. Wang, L. Ma, T. Li, M. Willander, Y. Jie, X. Cao and Z. L. Wang, *Adv. Energy Mater.*, 2016, **6**, 1501778.
3. Z. Li, J. Chen, J. Zhou, L. Zheng, K. C. Pradel, X. Fan, H. Guo, Z. Wen, M.-H. Yeh, C. Yu and Z. L. Wang, *Nano Energy*, 2016, **22**, 548-557.
4. G. Zhu, J. Chen, T. Zhang, Q. Jing and Z. L. Wang, *Nat. Commun.*, 2014, **5**, 3426.
5. M. M. Apodaca, P. J. Wesson, K. J. Bishop, M. A. Ratner and B. A. Grzybowski, *Angew. Chem. Int. Ed.*, 2010, **49**, 946-949.
6. H. Ryu, J.-H. Lee, T.-Y. Kim, U. Khan, J. H. Lee, S. S. Kwak, H.-J. Yoon and S.-W. Kim, *Adv. Energy Mater.*, 2017, **7**, 1700289.
7. S. Soh, H. Liu, R. Cademartiri, H. J. Yoon and G. M. Whitesides, *J. Am. Chem. Soc.*, 2014, **136**, 13348-13354.